

Post-Hoc Concept Disentanglement: From Correlated to Isolated Concept Representations

Eren Erogullari¹, Sebastian Lapuschkin^{1,2,†}, Wojciech Samek^{1,3,4,†}, Frederik Pahde^{1,†}

¹Fraunhofer Heinrich Hertz Institut, Berlin, Germany

²Centre of eXplainable Artificial Intelligence, Technological University Dublin

³Technische Universität Berlin, Berlin, Germany

⁴Berlin Institute for the Foundations of Learning and Data (BIFOLD), Berlin, Germany

†corresponding authors: {sebastian.lapuschkin,wojciech.samek,frederik.pahde}@hhi.fraunhofer.de

Abstract

Concept Activation Vectors (CAVs) are widely used to model human-understandable concepts as directions within the latent space of neural networks. They are trained by identifying directions from the activations of concept samples to those of non-concept samples. However, this method often produces similar, non-orthogonal directions for correlated concepts, such as “beard” and “necktie” within the CelebA dataset, which frequently co-occur in images of men. This entanglement complicates the interpretation of concepts in isolation and can lead to undesired effects in CAV applications, such as activation steering. To address this issue, we introduce a post-hoc concept disentanglement method that employs a non-orthogonality loss, facilitating the identification of orthogonal concept directions while preserving directional correctness. We evaluate our approach with real-world and controlled correlated concepts in CelebA and a synthetic FunnyBirds dataset with VGG16 and ResNet18 architectures. We further demonstrate the superiority of orthogonalized concept representations in activation steering tasks, allowing (1) the *insertion* of isolated concepts into input images through generative models and (2) the *removal* of concepts for effective shortcut suppression with reduced impact on correlated concepts in comparison to baseline CAVs.¹

¹Code is available at <https://github.com/erenerogullari/cav-disentanglement>

1 Introduction

With the growing reliance on deep learning in critical domains, such as applications in medicine [8] or criminal justice [48, 44], the need for eXplainable Artificial Intelligence (XAI) has become more relevant to ensure transparency and trust in model’s decision-making processes. XAI methods can be broadly categorized into local approaches, explaining individual predictions by attributing importance scores to input features (*e.g.*, [4, 37, 25]), and global approaches, aiming to uncover broader decision-making patterns learned by a model (*e.g.*, [21, 1, 14]). As such, concept-based explanations seek to represent abstract, human-understandable concepts in the model’s latent space, offering insights into how these concepts influence predictions. Specifically, Concept Activation Vectors (CAVs) allow interpreting Deep Neural Networks (DNNs) by modeling high-level concepts as directions in latent space [21]. They are typically learned using linear classifiers, *e.g.*, linear Support Vector Machines (SVMs), to separate activations corresponding to the presence vs absence of a concept, represented by the normal to the decision hyperplane of the classifier. However, while this approach optimizes the directional correctness of *individual* concepts, it may fail to isolate a concept’s direction from others when multiple correlated concepts are trained simultaneously. This is caused by highly entangled neural representations [13], *i.e.*, multiple concepts being encoded along overlapping directions due to correlations present in the dataset. This entanglement manifests in latent space as non-

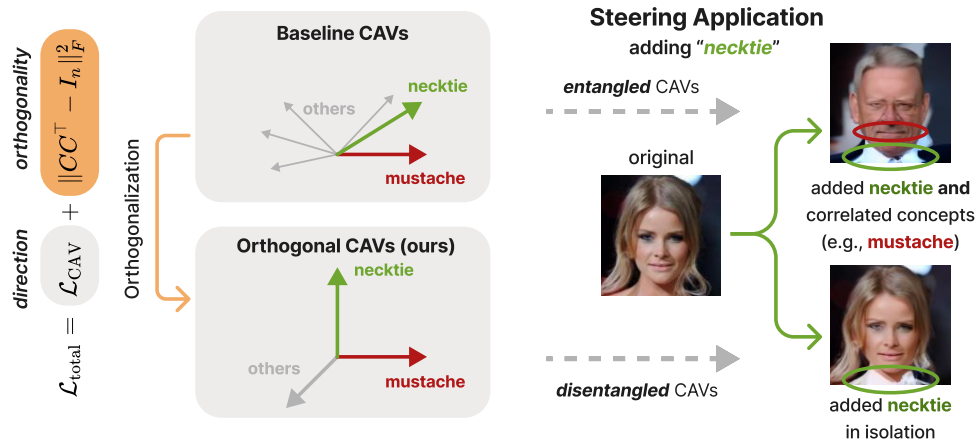


Figure 1: *Left*: Our novel CAV objective encourages the orthogonalization of multiple concept directions trained simultaneously. *Right*: The resulting disentangled CAVs are beneficial for various CAV applications, as concepts can be targeted in isolation. For example, when inserting the “necktie” concept to an input image in a steering task, the usage of *entangled* baseline CAVs might add correlated concepts as well (e.g., “mustache”), while *disentangled* CAVs add the targeted concept in isolation.

orthogonal concept directions [28], making it challenging to isolate individual concepts and leading to ambiguity and less interpretability in CAV-based explanations. For example, CAV-based steering applications, attempting to add [33] or remove [3] specific concepts, may unintentionally modify other entangled concepts, as illustrated in Fig. 1 (*top right*).

To tackle this issue holistically, we propose a novel CAV training objective penalizing non-orthogonality between concept directions trained simultaneously, thereby encouraging disentangled representations in latent space (Fig. 1, *left*). Our proposed loss term can be utilized in conjunction with any objective targeting directional correctness in a weighted manner to balance the trade-off between both optimization goals. We further introduce targeted orthogonalization, allowing to selectively enforce separation between specific concept pairs.

We evaluate our post-hoc concept orthogonalization approach through both controlled and real-world experiments using the CelebA and FunnyBirds datasets with VGG16 and ResNet18 architectures. Furthermore, we demonstrate the effectiveness of reduced concept entanglement in activation steering

applications. This includes (1) the insertion of isolated concepts in latent encodings of contemporary Diffusion models as shown in Fig. 1 (*bottom right*) and (2) the precise concept removal for shortcut suppression with minimal impact on correlated concepts. We compare orthogonalized CAVs to baseline CAVs trained in isolation and provide both qualitative and quantitative results.

2 Related Work

Existing works either interpret concepts as individual neurons [1, 29], higher-dimensional subspaces [45], or linear directions within the latent space [26, 21, 31, 9]. The latter provides a flexible way to capture representations by interpreting them as superpositions of multiple neurons [13]. Matrix factorization methods, such as non-negative matrix factorization, can be utilized to extract meaningful basis components in an unsupervised manner that act as interpretable concepts [14, 49]. We adopt the linear-directions paradigm and interpret concepts as linear directions learned in a supervised manner from latent model ac-

tivations. As many concept-based methods, such as steering methods for concept insertion or suppression, scale to multiple concepts, ensuring that learned directions remain disentangled becomes crucial to avoid interfering concepts.

Concept disentanglement methods can generally be categorized into (1) approaches utilized before or during model training, aiming to learn disentangled representations from the beginning, and (2) post-hoc disentanglement approaches, focusing on disentangling already learned but entangled concepts. Pre- or during-training strategies introduce constraints like whitening layers to ensure concept disentanglement across model’s layers [10], leverage metadata to separate relevant features from biases [35], or focus on learning disentangled representations of the underlying concepts in the data [46], either in a supervised [7, 43] or in an unsupervised manner [39, 19, 22]. Post-hoc methods, on the other hand, typically extend classic dimensionality-reduction techniques like Principal Component Analysis (PCA) or Independent Component Analysis (ICA) [11] to uncover disentangled directions from pretrained models without altering their original training pipelines. In contrast to other methods, we introduce a *supervised post-hoc* concept disentanglement approach by extending CAVs [21, 31] to enforce orthogonal concept directions within the latent space.

3 Post-Hoc Concept Orthogonalization

Notation. Given a neural network $f : \mathcal{X} \rightarrow \mathcal{Y}$ that maps input samples $\mathbf{x} \in \mathcal{X}$ to target labels $y \in \mathcal{Y}$, we can decompose the network into two functions $f = h \circ g$, with feature extractor $g : \mathcal{X} \rightarrow \mathcal{Z}$ with $\mathcal{Z} \subseteq \mathbb{R}^m$ mapping input samples to hidden layer activations $\mathbf{z} \in \mathcal{Z}$ at a given layer with m neurons, and classifier $h : \mathcal{Z} \rightarrow \mathcal{Y}$ mapping hidden layer activations to target labels y . Furthermore, given $n \in \mathbb{N}$ concepts with binary concept labels $\mathbf{t}^{(i)} \in \{-1, 1\}^n$ for each sample $\mathbf{x}^{(i)} \in \mathcal{X}$, the set of latent activations \mathcal{Z} of samples can be partitioned into two sets for each concept c with $\mathcal{Z} = \mathcal{Z}_c^+ \cup \mathcal{Z}_c^-$, where

$\mathcal{Z}_c^+ := \{g(\mathbf{x}^{(i)}) \mid \mathbf{x}^{(i)} \in \mathcal{X} \text{ and } t_c^{(i)} = 1\}$ is the set of activations with the target concept c , and $\mathcal{Z}_c^- := \{g(\mathbf{x}^{(i)}) \mid \mathbf{x}^{(i)} \in \mathcal{X} \text{ and } t_c^{(i)} = -1\}$ is the set of activations without the target concept. Whereas the choice of layer is problem-specific, in practice, commonly the penultimate layer is used, as research suggests that later layers have higher receptive fields and capture more complex and abstract concepts [6, 29, 34].

3.1 Concept Modeling via Concept Activation Vectors

CAVs are defined as the direction in latent space pointing from activations of samples *without* the target concept \mathcal{Z}^- to activations of samples *with* the target concept \mathcal{Z}^+ [21]. Most commonly, they are obtained from the weight vector $\mathbf{w} \in \mathbb{R}^m$ of a linear classifier [16, 47], *i.e.*, the hyperplane separating latent activations of these sample sets, some of which are linear SVMs minimizing the hinge loss with L2 regularization [12] and logistic, or ridge regression models minimizing the squared error loss with L2 regularization [20]. By finding the optimal classification boundary, linear classifiers aim to achieve the directional correctness of concepts.

Given $k = |\mathcal{X}| \in \mathbb{N}$ samples, a concept c , and a simple linear model $f_{\text{lin}}(\mathbf{z}) = \mathbf{w}^T \mathbf{z} + b$ with weight vector $\mathbf{w} \in \mathbb{R}^m$ and bias $b \in \mathbb{R}$ as the classifier along with a ridge regression term, we typically obtain the objective function

$$\arg \min_{\mathbf{w}, b} \mathcal{L}(\mathcal{Z}; \mathbf{w}, b) = \arg \min_{\mathbf{w}, b} \|\mathbf{t} - Z\mathbf{w} - \mathbf{b}\|_2^2 + \|\mathbf{w}\|_2^2 \quad (1)$$

with $\mathbf{t} \in \{-1, 1\}^k$ representing the label vector with concept label $t_c^{(i)}$ as the i^{th} element, $\mathbf{b} \in \mathbb{R}^k$ as an n -wise repetition of b , and $Z \in \mathbb{R}^{k \times m}$ as the input matrix with latent activations $\mathbf{z}^{(i)} \in \mathbb{R}^m$ on its rows.

Eq. (1) aims to find a weight that maximizes class-separability, which is prone to capturing distractor components that arise from noise and unrelated features in the data [16]. To address this, Pahde et al. [31] introduce Pattern-CAVs, assuming a linear dependency between the activations and the concept

labels and aiming to find a pattern that explains Z w.r.t concept labels \mathbf{t} , where the objective becomes

$$\arg \min_{\mathbf{w}, \mathbf{b}} \mathcal{L}_{\text{CAV}}(Z; \mathbf{w}, \mathbf{b}) = \arg \min_{\mathbf{w}, \mathbf{b}} \|Z - \mathbf{t}\mathbf{w}^T - \mathbf{b}\|_2^2 \quad (2)$$

leading to a solution invariant under feature scaling and more robust to noise.

However, both perspectives optimize CAVs in isolation and independent of other concepts, such that concept directions have no impact on other CAVs. This can result in solutions where CAVs share similar orientations and become entangled due to existing correlations in the training data. Throughout this paper, we will utilize Pattern-CAVs, as defined in Eq. (2), as the *baseline* CAVs.

3.2 Measuring Concept Entanglement

We consider concepts as entangled if their CAVs share similar orientations within the latent space, which can be analyzed empirically by their cosine similarity matrix. The cosine similarity between two vectors measures their angular similarity and, given two CAVs \mathbf{c}_i and \mathbf{c}_j , is defined as

$$\cos(\mathbf{c}_i, \mathbf{c}_j) = \frac{\mathbf{c}_i \cdot \mathbf{c}_j}{\|\mathbf{c}_i\| \|\mathbf{c}_j\|} \quad (3)$$

where values near 1 indicate high alignment, *i.e.*, entanglement, between the concepts, values near -1 indicate a strong inverse correlation or opposing directions in the feature space, and values near 0 suggest orthogonality and independence. The resulting matrix $C = (C_{ij}) = (\cos(\mathbf{c}_i, \mathbf{c}_j))$ provides insight into concept entanglement, where highly similar concepts may occupy overlapping regions in latent space. To quantify the orthogonality of a given concept to all others, we use the average cosine similarity, effectively describing the orthogonality of a concept in terms of a single metric, defined in Eq. (4).

An example for highly entangled concepts is shown in Fig. 2, where we show the CAVs trained on the CelebA dataset [24], consisting of images of celebrity faces with concept level annotations, such as “beard”,

“mustache”, and “makeup”. The resulting cosine similarity matrix of CAVs contains naturally emerging entanglement blocks, where different sets of concepts point in similar or opposite directions. This entanglement typically arises from the training of individual concepts in isolation without any information on other concepts, such that correlations in the dataset, *e.g.*, concepts that frequently appear together (*e.g.*, “beard” and “mustache”) or those that do not (*e.g.*, “mustache” and “makeup”), cause CAVs to align in similar or opposite directions in the latent space.

Orthogonality Metric. Given a finite set \mathcal{C} of concepts, we define the *orthogonality* O_i of a concept $\mathbf{c}_i \in \mathcal{C}$ as:

$$O_i = 1 - \frac{1}{|\mathcal{C}| - 1} \sum_{\tilde{\mathbf{c}} \in \mathcal{C} \setminus \{\mathbf{c}_i\}} |\cos(\mathbf{c}_i, \tilde{\mathbf{c}})| \quad (4)$$

where $|\cdot|$ is the absolute value function. Consequently, the value of O_i ranges between 0 and 1, where 1 represents perfect disentanglement and orthogonality of the given concept, and 0 represents complete entanglement and alignment with other concepts, sharing the same orientation in the latent space. We further define *average orthogonality* \bar{O} as the average of all concepts’ orthogonality values and use it as an indicator of overall disentanglement of concepts.

3.3 Orthogonalization of CAVs

Given a hidden layer with $m \in \mathbb{N}$ neurons and a finite set of concepts \mathcal{C} present in the dataset with $n = |\mathcal{C}|$ concepts, and further assuming a setting where the dimensionality of the latent space is significantly higher than the number of concepts, *i.e.*, when $m \gg n$, there is sufficient room for CAVs to be orthogonal to one another. Therefore, to disentangle concept representations, we propose an additional loss term, encouraging orthogonality between CAVs in latent space. Specifically, we define the orthogonality loss $\mathcal{L}_{\text{orth}}$ as

$$\mathcal{L}_{\text{orth}} = \|CC^T - I_n\|_F^2 \quad (5)$$

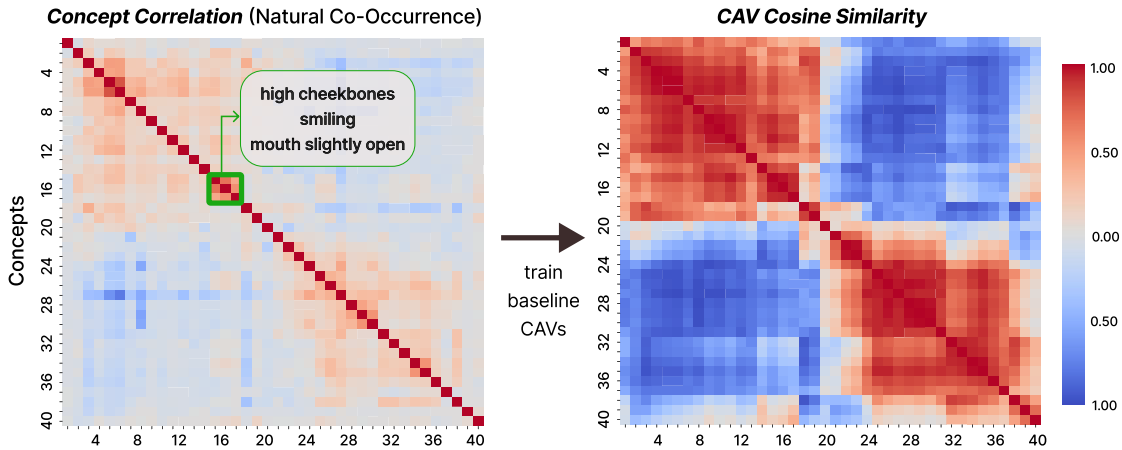


Figure 2: *Left*: Correlations of known concepts based on their co-occurrence in CelebA. *Right*: Pair-wise cosine similarities between concept representations via CAVs trained in isolation. Concepts frequently co-occurring in the training data (e.g., “high cheekbones”, “smiling”, and “mouth slightly open”) result in highly similar and entangled CAVs.

where $C \in \mathbb{R}^{n \times m}$ is the matrix of n CAVs with each row corresponding to a CAV, I_n is the n -dimensional identity matrix and $\|\cdot\|_F^2$ denotes the squared Frobenius norm. This loss term penalizes the deviation of the pair-wise cosine similarity matrix CC^\top from the identity matrix I_n , effectively encouraging the CAVs to be orthogonal. The orthogonality loss $\mathcal{L}_{\text{orth}}$ can be combined with the original loss term \mathcal{L}_{CAV} (e.g., in Eq. (2)) in a weighted manner as:

$$\mathcal{L} = \mathcal{L}_{\text{CAV}} + \alpha \mathcal{L}_{\text{orth}} \quad (6)$$

yielding the minimization objective with weighting parameter $\alpha > 0$ balancing the trade-off between the potentially competing goals to (1) maximize directional correctness with \mathcal{L}_{CAV} and (2) orthogonalize the CAVs with $\mathcal{L}_{\text{orth}}$. With $\alpha = 0$ the optimization objective becomes the original objective, which does not penalize the concept entanglement, whereas with $\alpha \rightarrow \infty$ the orthogonality term will dominate the loss and the optimization will most likely yield random orthogonal concept directions that fail at directional correctness.

In practice, our novel training objective can either be employed to optimize CAVs from random initial-

ization or to disentangle pre-trained CAVs in a fine-tuning step. While the former can balance the directional correctness objective and the orthogonality constraint from the beginning, it may require more iterations for convergence. The latter approach can lead to faster convergence, however, the magnitude of α must be chosen carefully to prevent over-correction by the orthogonality term. Finally, the average orthogonality \bar{O} can be used as a global metric to measure overall orthogonality of CAVs during optimization.

3.4 Targeted Orthogonalization with Weighted Penalization

While orthogonalization of all CAVs is beneficial, not all concepts require the same level of adjustment. For example, already disentangled concepts, *i.e.*, minimally correlated concepts, should remain largely unaffected, while entangled concepts should be prioritized. To achieve this, we introduce a symmetric weighting matrix $W_\beta \in \mathbb{R}^{n \times n}$ to adjust the weighting of concept pairs given a set of target pairs \mathcal{T} , resulting in the β -weighted orthogonalization loss $\mathcal{L}_{\text{orth}}^\beta$

defined as:

$$\mathcal{L}_{\text{orth}}^\beta = \|W_\beta \odot (CC^\top - I_n)\|_F^2 \quad (7)$$

where

$$(W_\beta)_{ij} = (W_\beta)_{ji} = \begin{cases} \beta & , \text{if } (i, j) \in \mathcal{T} \\ 1 & , \text{otherwise.} \end{cases} \quad (8)$$

where $\beta \in \mathbb{R}$ with $\beta > 0$ describing the relative importance of target pairs over non-target pairs and \odot denoting the Hadamard (element-wise) product. Having $\beta > 1$ will enforce a stricter disentanglement on the target pairs, while having $0 < \beta < 1$ will effectively relax the orthogonality constraint. Plugging the new $\mathcal{L}_{\text{orth}}^\beta$ loss in to Eq. (6) yields a new optimization objective, penalizing non-orthogonality of selected pairs of concepts over the others. This formulation allows selective penalization, focusing on disentangling specific pairs of highly entangled concepts while leaving already disentangled pairs largely unaffected. Note, that this formulation can easily be extended to individual weights for each pair, *i.e.* different values for each entry in W_β , while keeping W_β symmetric. In practice, target pairs can be defined as a list of most entangled pairs with high correlations or high cosine similarities.

3.5 Practical Implications: Directional Correctness and Orthogonality Trade-off

In order to maximize concept orthogonality while maintaining directional correctness, we monitor the macro-averaged Area Under Receiver Operating Curve (AUROC)², as a proxy metric for directional correctness, together with average orthogonality. Monitoring AUROC allows to ensure that the optimization does not compromise the primary goal of CAVs. We can further use AUROC to define an early-exit criteria, *e.g.*, thresholds based on the average AUROC, average-drop of AUROC, or max-drop

²Note, that although our CAVs are *not* computed as predictors, their dot products with latent activations can be used to measure the concept separability.

of AUROC. This ensures that the concept disentanglement preserves the directional correctness by preventing over-optimization at the expense of predictive performance, ensuring the CAVs remain useful for their intended purpose.

4 Experiments

We empirically evaluate our post-hoc concept disentanglement methods using real-world concepts in CelebA and controlled concepts in the synthetic FunnyBirds dataset. Specifically, our experiments investigate whether our approach can successfully disentangle CAV-based concept representations while preserving the directional correctness measured via their AUROC as a proxy metric.

4.1 Experiment Details

We conduct experiments with the real-world CelebA dataset [24] and the synthetic FunnyBirds dataset [18]. The former consists of images of faces along with binary concept labels for 40 attributes (see Appendix A for details). We consider the task of classifying samples with and without “blond hair”. Fig. 2 (*left*) presents the correlation matrix between these attributes, revealing two distinct blocks that reflect natural groupings of concepts associated with male and female attributes. Moreover, we utilize a synthetic dataset with generated images of 50 bird classes with part-level annotations for 5 body parts (beak, eye, foot, tail, and wing), which are transformed into binary concept labels (see Appendix B for details). We inject controlled correlations between “beak” and “tail” concepts, such that 70% of samples with a given beak type have a specific corresponding tail type. For example, beak type “beak01.glb” has a 70% probability of being paired with tail type “tail01.glb”, while the remaining 30% is split equally between the other tail types. This pattern is similarly applied to other beak types, resulting in controlled correlations between these concept attributes. For both datasets, we train VGG16 [38] and ResNet18 [17] models and train CAVs using

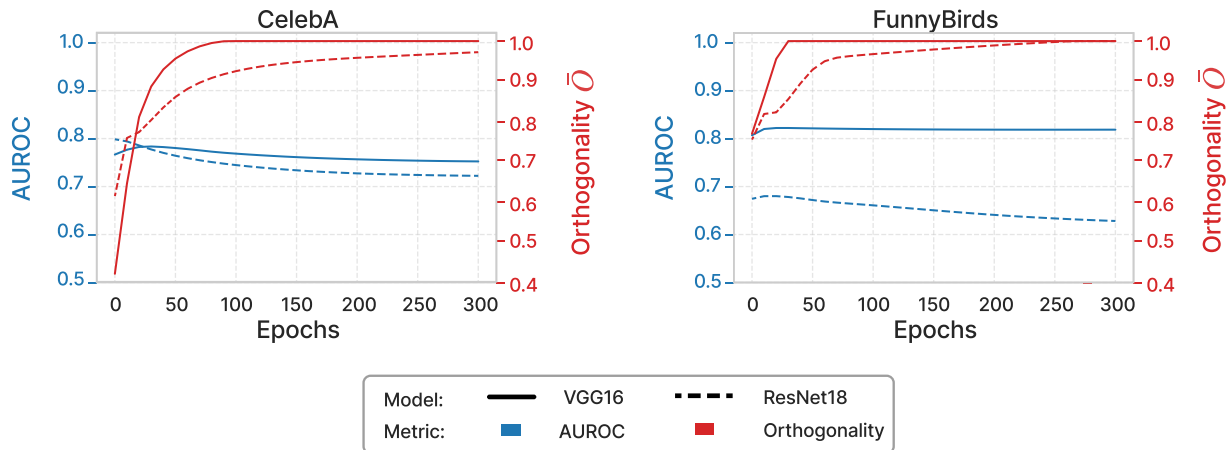


Figure 3: Evolution of AUROC (*blue*) and average orthogonality \bar{O} (*red*) during CAV optimization for ResNet18 and VGG16 models trained on CelebA (*left*) and FunnyBirds (*right*). Our approach achieves near-perfect orthogonalization, while preserving directional correctness as measured via AUROC.

activations from the last convolutional layers of both models.

4.2 Concept Disentanglement

To measure the orthogonality of CAVs and directional correctness during the proposed optimization procedure, we (1) monitor the per-concept orthogonality O_i , average orthogonality \bar{O} , as well as per-concept and macro-averaged AUROC during optimization and (2) compare the cosine similarity matrices between CAVs before and after optimization. In both experimental settings we optimize CAVs starting from both random and pre-trained initializations, *i.e.*, the solution for Eq. (2), and apply orthogonalization, as defined in Eq. (6).

Orthogonalization and Directional Correctness. First, we evaluate our proposed optimization objective on all datasets using both models. We fine-tune pre-trained CAVs for 300 epochs (see Appendix C for details). The results are shown in Fig. 3. Across all experiments, we observe a drastic increase in orthogonality, with CAVs achiev-

ing either near-perfect or complete orthogonalization within 300 epochs. This strong shift towards orthogonality indicates that our method effectively promotes concept disentanglement, ensuring that learned representations become more independent.

We further observe that, while enforcing orthogonality, directional correctness – measured via AUROC as a proxy metric – remains largely preserved. This indicates that the orthogonalization of CAVs only minimally harms their primary objective. Notably, in most experiments AUROC exhibits an initial increase at the beginning of optimization before undergoing a gradual decay and finally stabilizing at a slightly lower level. The initial increase in AUROC is likely due to the orthogonality constraint, which provides the optimization with a term that helps CAVs to be optimized jointly, as opposed to the baseline objective where each CAV is optimized separately. This encourages a better use of latent space via a more structured adjustment of CAVs. Overall, our results demonstrate that concept disentanglement can be effectively achieved without compromising directional correctness, making this approach robust across various settings.

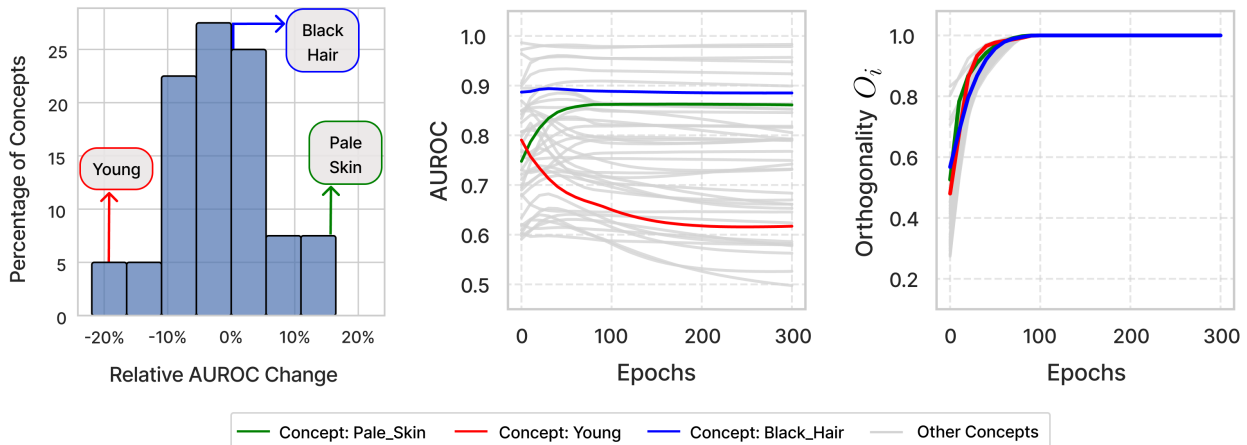


Figure 4: *Left*: Distribution of relative AUROC change before and after CAV optimization for the VGG16 model for CelebA. *Middle and Right*: Evolution of per-concept metrics orthogonality O_i and AUROC. We highlight concepts with the highest increase (*green*), the highest decrease (*red*), and the smallest change in AUROC (*blue*).

Concept Dynamics Under Orthogonalization.

As certain concepts are initially more entangled than others, different CAVs undergo different directional changes in the latent space. In order to get an insight into how individual directional changes happen, and how these changes affect the performance of individual concepts, we provide an in-depth analysis of the orthogonality and AUROC metrics of individual concepts during CAV optimization. Here, we fine-tune CAVs trained on the VGG16 model for the CelebA dataset.

Fig. 4 illustrates the changes in AUROC and orthogonality of each CAV during optimization. Out of all concepts present in the CelebA dataset, we highlight three, namely the concept with the highest increase (“Pale Skin”), highest decrease (“Young”), and least change in AUROC (“Black Hair”). We observe that while all concepts increase in orthogonality during optimization, some experience an improvement, while others suffer from a decline in their classification performance. Furthermore, although some concepts maintain a relatively stable AUROC performance, e.g. concept with blue line on Fig. 4, they still

experience an increase in orthogonality, either due to the fact that they change their direction without losing their classification performance, or that other entangled concepts move away from the concept, such that it becomes more orthogonal to them.

The dynamics of entangled concepts during optimization is further highlighted in Fig. 5, where we show the AUROC change distribution of two different sets of entangled concepts before and after the optimization on the CelebA dataset starting from an optimal state for CAVs. The sets are chosen from the initial cosine similarity matrix of CAVs that are optimized without any orthogonalization, where we observe a naturally emergent blocks due to correlations in dataset associated with female- and male-related concepts. The resulting AUROC change distribution shows that in each entanglement block, there are concepts that experience an increase in AUROC, concepts that suffer from a decrease in AUROC, and concepts that are relatively stable in terms of AUROC, which is a clear indication that CAVs undergo a redistribution of representational importance. Some concepts sacrifice their distinctiveness or classifica-

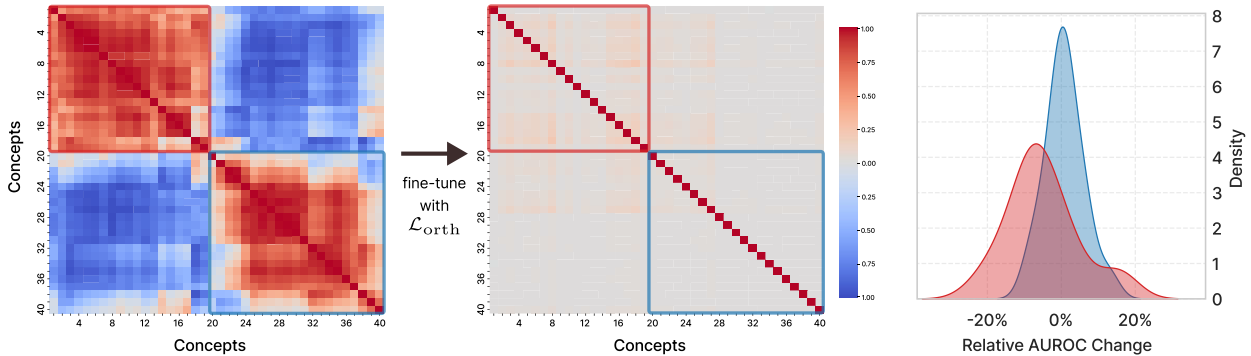


Figure 5: *Left and Middle*: Cosine similarity matrices of CAVs, trained on VGG16 model on CelebA dataset, before and after the fine-tuning. *Right*: Kernel Density Estimation of relative AUROC changes of individual concepts in two entangled blocks of female- (*red*) and male-associated (*blue*) concepts.

tion ability to reduce redundancy and entanglement, while others gain clarity and improved directional correctness as a result of orthogonalization. Fig. 5 further depicts a global image of concept orthogonalization in latent space, where we consider the cosine similarity matrices of CAVs before and after the optimization. The resulting cosine similarity matrix after orthogonalization illustrates the achievement of the secondary goal of optimization, *i.e.*, concept disentanglement, as it resembles the identity matrix, which was the desired root point of $\mathcal{L}_{\text{orth}}$ defined in Section 3.3. Similar results are obtained for the Funny-Birds dataset, as shown in Appendix B.

Impact of Weighting Parameter α . We measure the orthogonality and AUROC of CAVs after optimization with our disentanglement loss introduced in Eq. (6) with various weightings $\alpha \in [10^{-10}, 10^{-9}, \dots, 10^{10}]$. We run the optimization for randomly initialized CAVs for the VGG16 model for CelebA with a learning rate of 0.1 and 500 epochs. The results are shown in Fig. 6, where the AUROC and orthogonality metrics are displayed for each value of the weighting parameter α . The results indicate that higher α values expectedly lead to a better level of orthogonalization and plateau when perfect orthogonalization is achieved. Interestingly, we ob-

serve that for small weighting parameters, the average AUROC slightly *increases* compared to the baseline CAVs without orthogonality constraint ($\alpha = 0$). This reflects the findings discussed in Section 4.2, *i.e.*, the joint optimization of *all* concept directions simultaneously can positively impact the directional correctness. However, with larger α values we observe a drastic drop in AUROC, indicating that the orthogonalization constraint outweighs the directional correctness objective. These results demonstrate the role of α to balance the trade-off between directional correctness, measured via AUROC, and the level of orthogonalization. Our results further indicate that optimal α values, where both AUROC and \bar{O} are maximized (here: values between 10^{-4} and 10^0), can (1) achieve perfect concept orthogonalization, and (2) refine directional correctness and achieve higher AUROC scores.

4.3 Disentanglement of Concept Heatmaps

Although evaluating concept disentanglement through orthogonality and AUROC metrics offer valuable insight into the quantitative performance of our method, they come short in providing a qualitative understanding of the underlying repre-

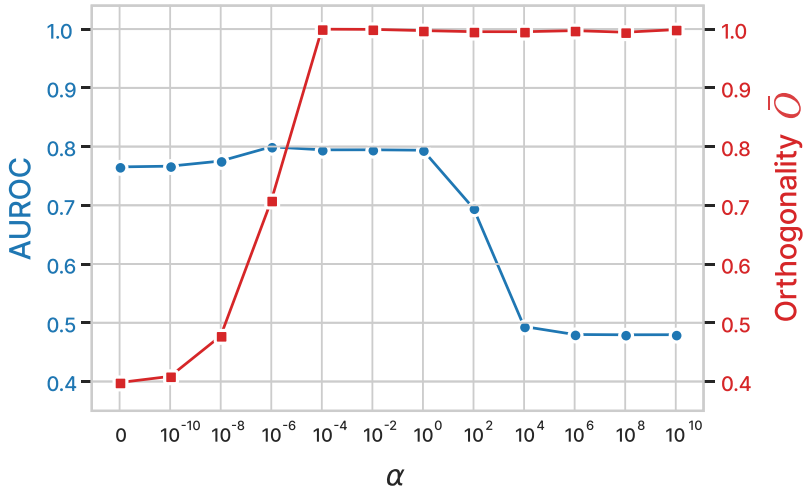


Figure 6: The average orthogonality \bar{O} and AUROC after CAV training on the last convolutional layer of VGG16 for CelebA. The x-axis represents the magnitude of α , while AUROC (blue) and orthogonality (red) are shown on the y1- and y2-axis, respectively.

sentational changes of concepts. To address this, we utilize Layer-wise Relevance Propagation (LRP) [4] to generate heatmaps for entangled concept pairs before and after orthogonalizing the CAVs using the `zennit` library [2]. More specifically, we compute the inner product between the activation of a sample and the CAV of interest, and then backpropagate the resulting relevances back to the input space [30, 3, 32]. Similarly, other attribution methods such as Guided Backpropagation [41], SmoothGrad [40], and Integrated Gradients [42] can be used to obtain such local explanations [9]. The heatmaps obtained from the VGG16 model, trained on the CelebA dataset, are illustrated in Fig. 7. The baseline CAVs successfully identify the regions associated with each concept; however, they show limitations in isolating the concepts entirely. Specifically, due to inherent correlations in the dataset, such as the high negative correlation observed between “blond hair” and “necktie” attributes, the heatmaps display negative relevance in each others regions that are unrelated to the original concept. In other words, the model tends to rely on the presence of one concept to indicate the absence of the other, or vice

versa. Conversely, following the orthogonalization of the CAVs, the heatmaps continue to accurately highlight the relevant regions, thereby demonstrating directional correctness, while substantially reducing the negative correlations and improving the isolation of individual concepts. This outcome indicates that CAVs obtained by our method not only effectively capture the relevant spatial regions within the input space but also achieve superior performance in disentangling and isolating the concepts.

5 CAV-based Activation Steering Applications

To evaluate the benefits of orthogonalized CAVs, we compare the results for CAV-based steering tasks using baseline CAVs without non-orthogonality penalization and orthogonalized CAVs. Specifically, we use CAVs to model concept directions in the latent space to either *insert* isolated concepts into input samples using generative models in qualitative experiments (Section 5.1), or to *remove* targeted concepts during inference time for shortcut suppression in a controlled

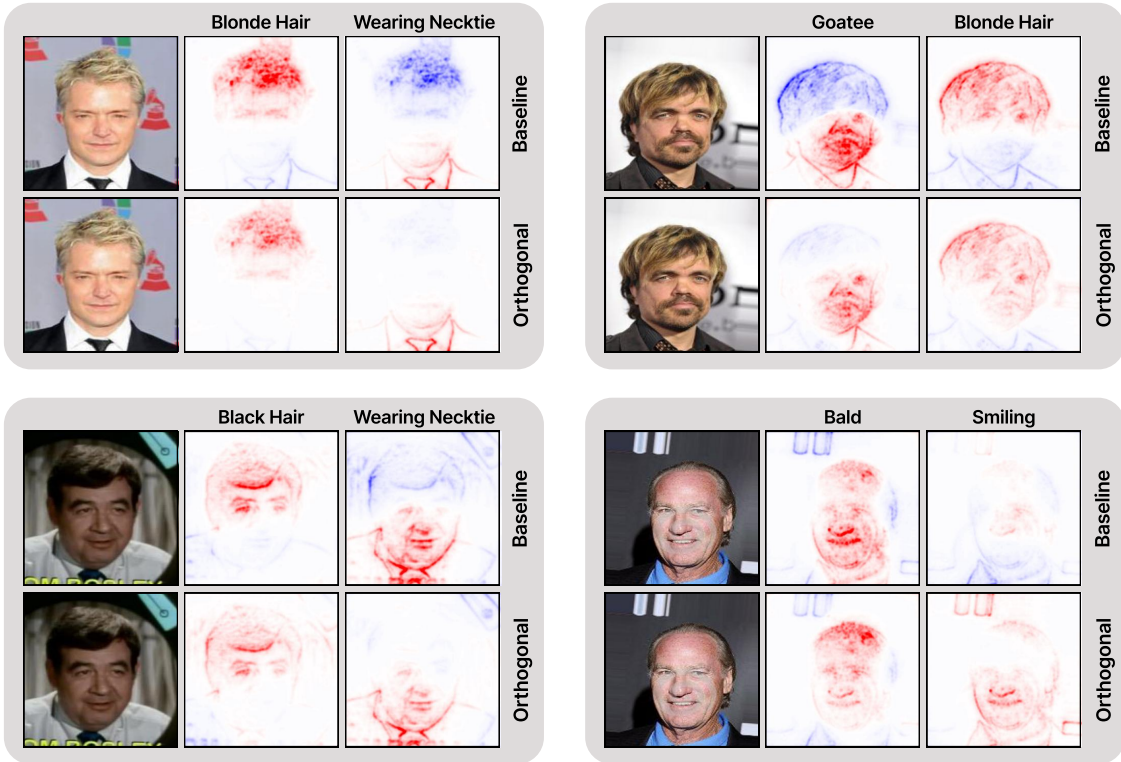


Figure 7: Concept heatmaps for 4 entangled pairs of concepts obtained using LRP on the VGG16 model for CelebA. For each pair, the three columns represent the original image (*left*) and the heatmaps corresponding to first (*middle*) and second (*right*) concept, respectively, whereas the rows represent the heatmaps obtained before and after CAV orthogonalization. Red and blue regions indicate positive and negative relevance.

scenario with both quantitative and qualitative results (Section 5.2).

5.1 Concept Insertion with Generative Models

As a first steering task, we consider the insertion of concepts by adding activations into the CAV direction. Intuitively, if precisely modeled, this corresponds to adding the concept to the input image. However, if concept representations are entangled, such as “wearing necktie” and “mustache” concepts in CelebA, adding activations along the CAV directions might lead to undesired effects. To investigate this qualitatively, we utilize a Diffusion Autoencoder [33]

trained on CelebA dataset. Diffusion Autoencoders are a class of generative models that learn structured latent representations by combining a learnable encoder with a diffusion-based decoder. Unlike traditional autoencoders, Diffusion Autoencoders separate the latent space into two components: a semantic subcode, which encodes high-level, structured information, and a stochastic subcode, which models low-level stochastic variations. This separation allows Diffusion Autoencoders to achieve both meaningful representation learning and high-level reconstruction capabilities, making them well-suited for activation steering applications. This allows the generation of images representing the manipulated encoding with added activations, *i.e.*, inserted concepts.

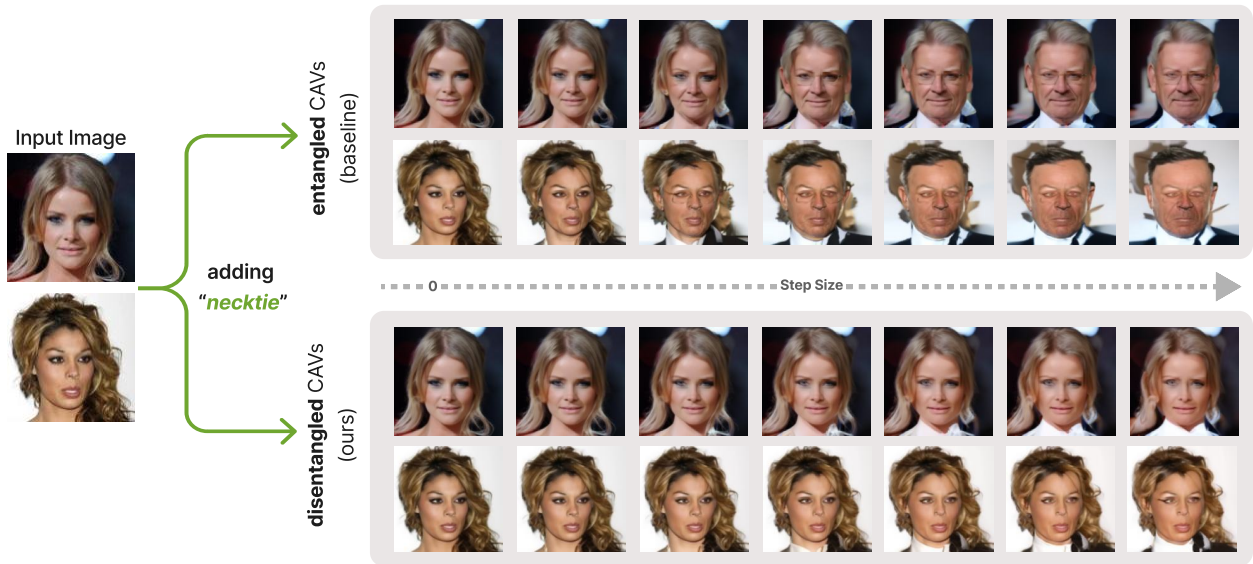


Figure 8: Given input images (*left*), we utilize a Diffusion Autoencoder to reconstruct manipulated latent encodings obtained at the bottleneck layer of the Diffusion Autoencoder. Specifically, we add activations with different step sizes into the concept direction for “necktie”, as modeled via baseline (*top*) and orthogonalized (*bottom*) CAVs. Whereas entangled baseline CAVs add correlated concepts in addition to the target concept, the disentangled CAV is capable of adding the “necktie” in isolation with minimized impact on other concepts.

We train both *baseline* and *orthogonalized* CAVs on the bottleneck layer of the Diffusion Autoencoder, using the pretrained model weights provided by the authors of [33]. Subsequently, we utilize the learned CAV for the concept “wearing necktie” to insert the target concept by adding activations along its direction with different step sizes. Lastly, we decode the manipulated encoding to obtain the corresponding images.

Fig. 8 illustrates the resulting images for both CAV directions over different step sizes. Both CAVs succeed in adding the desired concept to given samples. However, the baseline CAV erroneously adds other *entangled* concepts, such as “mustache” and “eyeglasses”, as a result of correlated concept directions. In contrast, the orthogonalized CAV shows superior results by adding the desired concept whilst avoiding the addition of correlated concepts. In addition, the results indicate that our proposed approach

generalizes well to larger models, such as Diffusion Autoencoders, demonstrating its scalability and effectiveness in more complex architectures.

5.2 Quantifying Collateral Damage: Concept Removal for Shortcut Suppression

Another popular steering task with CAVs is the removal of undesired concepts for the suppression of shortcut behavior. Shortcuts can be caused by spurious correlations in the training data, where concepts (causally) unrelated to the task correlate with the target label [15]. Post-hoc model editing approaches for shortcut suppression utilize concept representations, such as CAVs, to model the undesired data artifact in latent space and suppress activations related to the concept during inference [36, 3, 27, 5]. However, model editing with entangled concept represen-

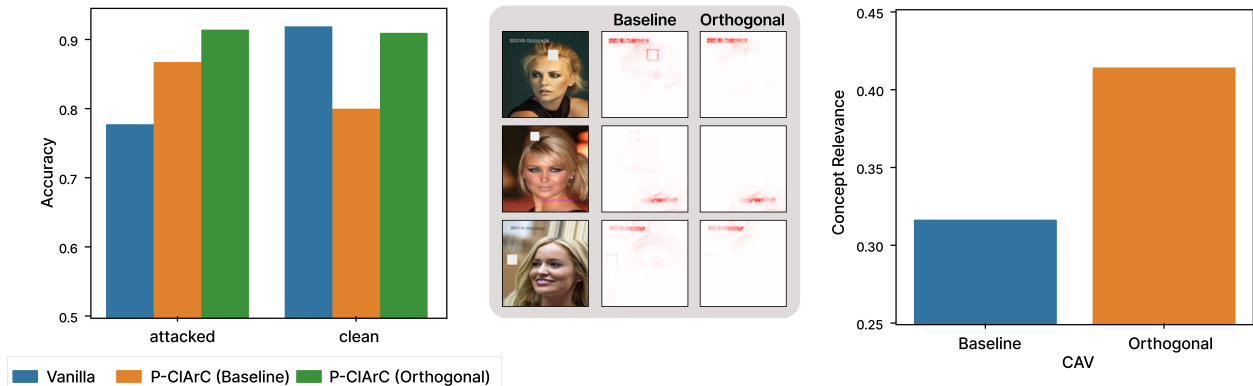


Figure 9: *Left*: Accuracy on clean and attacked test sets for the Vanilla model and P-CIArC-corrected models using baseline- and orthogonal-CAVs. The latter achieves a higher robustness towards the artifact and less collateral damage. *Middle*: Concept heatmaps for the timestamp. *Right*: Percentage of relevance for concept heatmaps on ground truth region. The orthogonal CAV localizes the concept more precisely.

tations can lead to collateral damage, as concepts entangled with the targeted concept are harmfully suppressed as well [23, 5]. In this experiment, we measure both the effectiveness of the shortcut suppression and the caused collateral damage for the model editing approach P-CIArC [3] which subtracts activations in the CAV direction at inference time. We compare the results for the baseline and orthogonalized CAVs in a controlled setting using artificial artifacts in CelebA. Specifically, we insert a “timestamp” as text overlay into 40% of samples of class “blonde” and only 0.5% of samples of class “non-blonde”, causing a spurious correlation between the “timestamp” and the class label. In addition, we insert a “white box” with varying size at random positions with probability 50% if there is a “timestamp” and 10% otherwise, leading to an entanglement between the concepts “timestamp” and “box”. We train a VGG16 model with stochastic gradient descent and a learning rate of 0.001, and expect the model to learn a shortcut based on the artificial correlation. To measure the model’s sensitivity towards the concept, we evaluate the performance on an attacked test set with the timestamp inserted into *all* samples. This distribution shift causes models utilizing the shortcut to perform poorly. Further, using a clean test set with *no*

artificial artifacts, allows evaluating the caused collateral damage. We compute baseline CAVs for the original 40 concepts, as well as the newly introduced concepts “box” and “timestamp”, using the Pattern-CAV defined in Eq. (2). For the concept disentanglement, we fine-tune the pre-trained CAVs with the orthogonalization loss in Eq. (7) with $\alpha = 1$, $\beta = 100$, and learning rate 0.0001 for 500 epochs.

The resulting classification performance on both test sets using the original model without shortcut suppression (*Vanilla*) and the models corrected via P-CIArC using *baseline* and *orthogonal* CAVs are shown in Fig 9 (*left*). The performance on the attacked test set is poor compared to the clean test set for the Vanilla model, confirming that the model uses the expected shortcut. Whereas the P-CIArC-corrected model using the baseline CAV performs slightly better on the attacked test set, the accuracy drops significantly on the clean test set due to collateral damage. In contrast, the model corrected via P-CIArC with the orthogonal CAV performs well on both test sets. In addition, Fig. 9 (*middle*) presents concept heatmaps using the timestamp CAVs as described in Sec. 4.3. Whereas the heatmap for the baseline CAV highlights the timestamp as well as

correlated concepts (*e.g.*, the “box”), the orthogonal CAV focuses on the timestamp in isolation. Lastly, quantifying these findings, Fig. 9 (*right*) shows the percentage of relevance on the ground truth region of the timestamp, confirming the visual findings that heatmaps computed using the orthogonal CAV provide a more accurate localization of the concept.

6 Conclusions and Future Work

In this work, we introduce a post-hoc concept disentanglement approach that utilizes a novel CAV training objective penalizing non-orthogonality while preserving directional correctness. We show the applicability of our loss term to find CAVs that are both meaningful and orthogonal with controlled and real-world concept correlations. We further demonstrate the benefits of orthogonalized concept directions for CAV-based steering tasks, allowing to add or remove concepts in isolation without impacting correlated concepts. Future research might focus on the semi-supervised training of CAVs to identify unlabeled concepts in addition or the definition of new training objectives allowing the joint training of multiple CAV directions. Moreover, the integration of our orthogonalization loss into the model training is a promising research direction.

Acknowledgements

This work was supported by the Federal Ministry of Education and Research (BMBF) as grant BIFOLD (01IS18025A, 01IS180371I); the European Union’s Horizon Europe research and innovation programme (EU Horizon Europe) as grants [ACHILLES (101189689), TEMA (101093003)]; and the German Research Foundation (DFG) as research unit DeSBI [KI-FOR 5363] (459422098).

References

[1] Reduan Achtiabat, Maximilian Dreyer, Ilona Eisenbraun, Sebastian Bosse, Thomas Wie-

gand, Wojciech Samek, and Sebastian Lapuschkin. From attribution maps to human-understandable explanations through concept relevance propagation. *Nature Machine Intelligence*, 5(9):1006–1019, 2023.

- [2] Christopher J Anders, David Neumann, Wojciech Samek, Klaus-Robert Müller, and Sebastian Lapuschkin. Software for dataset-wide xai: from local explanations to global insights with zennit, corelay, and virelay. *arXiv preprint arXiv:2106.13200*, 2021.
- [3] Christopher J Anders, Leander Weber, David Neumann, Wojciech Samek, Klaus-Robert Müller, and Sebastian Lapuschkin. Finding and removing clever hans: Using explanation methods to debug and improve deep models. *Information Fusion*, 77:261–295, 2022.
- [4] Sebastian Bach, Alexander Binder, Grégoire Montavon, Frederick Klauschen, Klaus-Robert Müller, and Wojciech Samek. On pixel-wise explanations for non-linear classifier decisions by layer-wise relevance propagation. *PloS one*, 10(7), 2015.
- [5] Dilyara Bareeva, Maximilian Dreyer, Frederik Pahde, Wojciech Samek, and Sebastian Lapuschkin. Reactive model correction: Mitigating harm to task-relevant features via conditional bias suppression. In *Proceedings of the IEEE/CVF Conference on Computer Vision and Pattern Recognition*, pages 3532–3541, 2024.
- [6] David Bau, Jun-Yan Zhu, Hendrik Strobelt, Agata Lapedriza, Bolei Zhou, and Antonio Torralba. Understanding the role of individual units in a deep neural network. *Proceedings of the National Academy of Sciences*, 117(48):30071–30078, 2020.
- [7] Diane Bouchacourt, Ryota Tomioka, and Sebastian Nowozin. Multi-level variational autoencoder: Learning disentangled representations from grouped observations. In *Proceedings of the AAAI Conference on Artificial Intelligence*, volume 32, 2018.

- [8] Titus J Brinker, Achim Hekler, Alexander H Enk, Joachim Klode, Axel Hauschild, Carola Berking, Bastian Schilling, Sebastian Haferkamp, Dirk Schadendorf, Tim Holland-Letz, et al. Deep learning outperformed 136 of 157 dermatologists in a head-to-head dermoscopic melanoma image classification task. *European Journal of Cancer*, 113:47–54, 2019.
- [9] Lennart Brocki and Neo Christopher Chung. Concept saliency maps to visualize relevant features in deep generative models. In *2019 18th IEEE international conference on machine learning and applications (ICMLA)*, pages 1771–1778. IEEE, 2019.
- [10] Zhi Chen, Yijie Bei, and Cynthia Rudin. Concept whitening for interpretable image recognition. *Nature Machine Intelligence*, 2(12):772–782, 2020.
- [11] Pattarawat Chormai, Jan Herrmann, Klaus-Robert Müller, and Grégoire Montavon. Disentangled explanations of neural network predictions by finding relevant subspaces. *IEEE Transactions on Pattern Analysis and Machine Intelligence*, 2024.
- [12] Corinna Cortes and Vladimir Vapnik. Support-vector networks. *Machine learning*, 20:273–297, 1995.
- [13] Nelson Elhage, Tristan Hume, Catherine Olsson, Nicholas Schiefer, Tom Henighan, Shauna Kravec, et al. Toy models of superposition. *arXiv preprint arXiv:2209.10652*, 2022.
- [14] Thomas Fel, Agustin Picard, Louis Bethune, Thibaut Boissin, David Vigouroux, Julien Colin, Rémi Cadène, and Thomas Serre. Craft: Concept recursive activation factorization for explainability. In *CVPR*, pages 2711–2721, 2023.
- [15] Robert Geirhos, Jörn-Henrik Jacobsen, Claudio Michaelis, Richard Zemel, Wieland Brendel, et al. Shortcut learning in deep neural networks. *Nat Mach Intell*, 2(11):665–673, 2020.
- [16] Stefan Haufe, Frank Meinecke, Jan Göcke, Stefan Dähne, J-D Haynes, Benjamin Blankertz, and Falk Bießmann. On the interpretation of weight vectors of linear models in multivariate neuroimaging. *NeuroImage*, 87:96–110, 2014.
- [17] Kaiming He, Xiangyu Zhang, Shaoqing Ren, and Jian Sun. Deep residual learning for image recognition. In *CVPR*, pages 770–778, 2016.
- [18] Robin Hesse, Simone Schaub-Meyer, and Stefan Roth. Funnybirds: A synthetic vision dataset for a part-based analysis of explainable ai methods. In *Proceedings of the IEEE/CVF International Conference on Computer Vision*, pages 3981–3991, 2023.
- [19] R. Devon Hjelm, Andrei Fedorov, Simon Lavoie-Marchildon, et al. Learning deep representations by mutual information estimation and maximization. In *Proceedings of the International Conference on Learning Representations (ICLR)*, 2019.
- [20] Arthur E Hoerl and Robert W Kennard. Ridge regression: Biased estimation for nonorthogonal problems. *Technometrics*, 42(1):80–86, 2000.
- [21] Been Kim, Martin Wattenberg, Justin Gilmer, Carrie Cai, James Wexler, Fernanda Viegas, et al. Interpretability beyond feature attribution: Quantitative testing with concept activation vectors (tcav). In *ICML*, pages 2668–2677. PMLR, 2018.
- [22] Hyunjik Kim and Andriy Mnih. Disentangling by factorising. In *ICML*, pages 2649–2658. PMLR, 2018.
- [23] Abhinav Kumar, Chenhao Tan, and Amit Sharma. Probing classifiers are unreliable for concept removal and detection. *Advances in Neural Information Processing Systems*, 35:17994–18008, 2022.
- [24] Ziwei Liu, Ping Luo, Xiaogang Wang, and Xiaoou Tang. Deep learning face attributes in the wild. In *Proceedings of International Conference on Computer Vision (ICCV)*, December 2015.

- [25] Scott M Lundberg and Su-In Lee. A unified approach to interpreting model predictions. *NeurIPS*, 30, 2017.
- [26] Neel Nanda, Andrew Lee, and Martin Wattenberg. Emergent linear representations in world models of self-supervised sequence models. In *Proceedings of the 6th BlackboxNLP Workshop: Analyzing and Interpreting Neural Networks for NLP*, pages 16–30, 2023.
- [27] Yannic Neuhaus, Maximilian Augustin, Valentin Boreiko, and Matthias Hein. Spurious features everywhere-large-scale detection of harmful spurious features in imagenet. In *ICCV*, 2023.
- [28] Angus Nicolson, Lisa Schut, J Alison Noble, and Yarin Gal. Explaining explainability: Understanding concept activation vectors. *TMLR*, 2025.
- [29] Chris Olah, Alexander Mordvintsev, and Ludwig Schubert. Feature visualization. *Distill*, 2(11), 2017.
- [30] Frederik Pahde, Maximilian Dreyer, Wojciech Samek, and Sebastian Lapuschkin. Reveal to revise: An explainable ai life cycle for iterative bias correction of deep models. In *MICCAI*, pages 596–606. Springer, 2023.
- [31] Frederik Pahde, Maximilian Dreyer, Leander Weber, Moritz Weckbecker, Christopher J Anders, Thomas Wiegand, Wojciech Samek, and Sebastian Lapuschkin. Navigating neural space: Revisiting concept activation vectors to overcome directional divergence. *arXiv preprint arXiv:2202.03482*, 2022.
- [32] Frederik Pahde, Thomas Wiegand, Sebastian Lapuschkin, and Wojciech Samek. Ensuring medical ai safety: Explainable ai-driven detection and mitigation of spurious model behavior and associated data. *arXiv preprint arXiv:2501.13818*, 2025.
- [33] Konpat Preechakul, Nattanat Chatthee, Suttisak Wizadwongsa, and Supasorn Suwajanakorn. Diffusion autoencoders: Toward a meaningful and decodable representation. In *CVPR*, pages 10619–10629, 2022.
- [34] Alec Radford, Rafal Jozefowicz, and Ilya Sutskever. Learning to generate reviews and discovering sentiment. *arXiv preprint arXiv:1704.01444*, 2017.
- [35] Alexander Rakowski, Remo Monti, Viktoriia Huryn, Marta Lemanczyk, Uwe Ohler, and Christoph Lippert. Metadata-guided feature disentanglement for functional genomics. *Bioinformatics*, 40, 2024.
- [36] Shauli Ravfogel, Yanai Elazar, Hila Gonen, Michael Twiton, and Yoav Goldberg. Null it out: Guarding protected attributes by iterative nullspace projection. In Dan Jurafsky, Joyce Chai, Natalie Schluter, and Joel Tetreault, editors, *ACL*, pages 7237–7256, July 2020.
- [37] Ramprasaath R Selvaraju, Michael Cogswell, Abhishek Das, Ramakrishna Vedantam, Devi Parikh, and Dhruv Batra. Grad-cam: Visual explanations from deep networks via gradient-based localization. In *ICCV*, pages 618–626, 2017.
- [38] Karen Simonyan and Andrew Zisserman. Very deep convolutional networks for large-scale image recognition. In Yoshua Bengio and Yann LeCun, editors, *ICLR 2015*, 2015.
- [39] Krishna Kumar Singh, Utkarsh Ojha, and Yong Jae Lee. Finegan: Unsupervised hierarchical disentanglement for fine-grained object generation and discovery. In *CVPR*, pages 6490–6499, 2019.
- [40] Daniel Smilkov, Nikhil Thorat, Been Kim, Fernanda Viégas, and Martin Wattenberg. Smoothgrad: removing noise by adding noise. *arXiv preprint arXiv:1706.03825*, 2017.
- [41] Jost Tobias Springenberg, Alexey Dosovitskiy, Thomas Brox, and Martin Riedmiller. Striving for simplicity: The all convolutional net. *arXiv preprint arXiv:1412.6806*, 2014.

- [42] Mukund Sundararajan, Ankur Taly, and Qiqi Yan. Axiomatic attribution for deep networks. In *ICML*, 2017.
- [43] Frederik Träuble, Elliot Creager, Niki Kilbertus, Francesco Locatello, Andrea Dittadi, Anirudh Goyal, Bernhard Schölkopf, and Stefan Bauer. On disentangled representations learned from correlated data. In *ICML*, pages 10401–10412. PMLR, 2021.
- [44] Guido Vittorio Travaini, Federico Pacchioni, Silvia Bellumore, Marta Bosia, and Francesco De Micco. Machine learning and criminal justice: A systematic review of advanced methodology for recidivism risk prediction. *International journal of environmental research and public health*, 19(17):10594, 2022.
- [45] Johanna Vielhaben, Stefan Bluecher, and Nils Strodthoff. Multi-dimensional concept discovery (mcd): A unifying framework with completeness guarantees. *TMLR*, 2023.
- [46] Xin Wang, Hong Chen, Zihao Wu, Wenwu Zhu, et al. Disentangled representation learning. *IEEE Transactions on Pattern Analysis and Machine Intelligence*, 2024.
- [47] Mert Yuksekgonul, Maggie Wang, and James Zou. Post-hoc concept bottleneck models. In *ICLR Workshops*, 2022.
- [48] Aleš Završnik. Algorithmic justice: Algorithms and big data in criminal justice settings. *European Journal of criminology*, 18(5), 2021.
- [49] Ruihan Zhang, Prashan Madumal, Tim Miller, Krista A Ehinger, and Benjamin IP Rubinstein. Invertible concept-based explanations for cnn models with non-negative concept activation vectors. In *Proceedings of the AAAI Conference on Artificial Intelligence*, volume 35, pages 11682–11690, 2021.

A CelebA Details

In this section we provide additional details on the CelebA dataset. Figure 10 presents the correlation and cosine similarity matrices for concepts extracted from the last convolutional layer of a VGG16 model trained on CelebA. The highlighted blocks in both matrices reveal two natural concept groups associated with female (*red*) and male (*blue*) attributes. The concept labels of these groups are listed in Table 3 using the same color coding for both entanglement blocks.

B FunnyBirds Details

Beak Model	tail01.glb	tail02.glb	tail03.glb
beak01.glb	0.7	0.15	0.15
beak02.glb	0.15	0.7	0.15
beak03.glb	0.15	0.15	0.7
beak04.glb	0.15	0.15	0.7

Table 1: Correlations between beak models and tail models based on enforced probabilities during dataset generation.

We provide details about the synthetic FunnyBirds dataset we generated for our experiments. In Table 1 we list the probabilities we used for the co-occurrence of concepts during the dataset generation to enforce correlations in the dataset, namely between *beak* and *tail* concepts. The resultant correlations, as well as the cosine similarity matrices before and after the CAV fine-tuning are illustrated in Fig. 12, where we fine-tune CAVs on the ResNet18 model trained on the FunnyBirds dataset (see Appendix C for more details). Finally, in Fig. 11 we display some example samples for the first 4 classes out of 50 total classes.

C CAV Training Details

Dataset	Model	LR	α	Epochs
CelebA	VGG16	0.001	0.01	300
	ResNet18	0.001	0.01	300
FunnyBirds	VGG16	0.001	0.1	300
	ResNet18	0.001	0.01	300

Table 2: Hyperparameters used for CAV fine-tuning. α denotes the weighting parameter used in Eq. (5).

In this section, we provide the hyperparameters used for training CAVs. Table 2 lists the learning rate, weighting parameter α and number of epochs used for fine-tuning CAVs for each dataset-model combination.

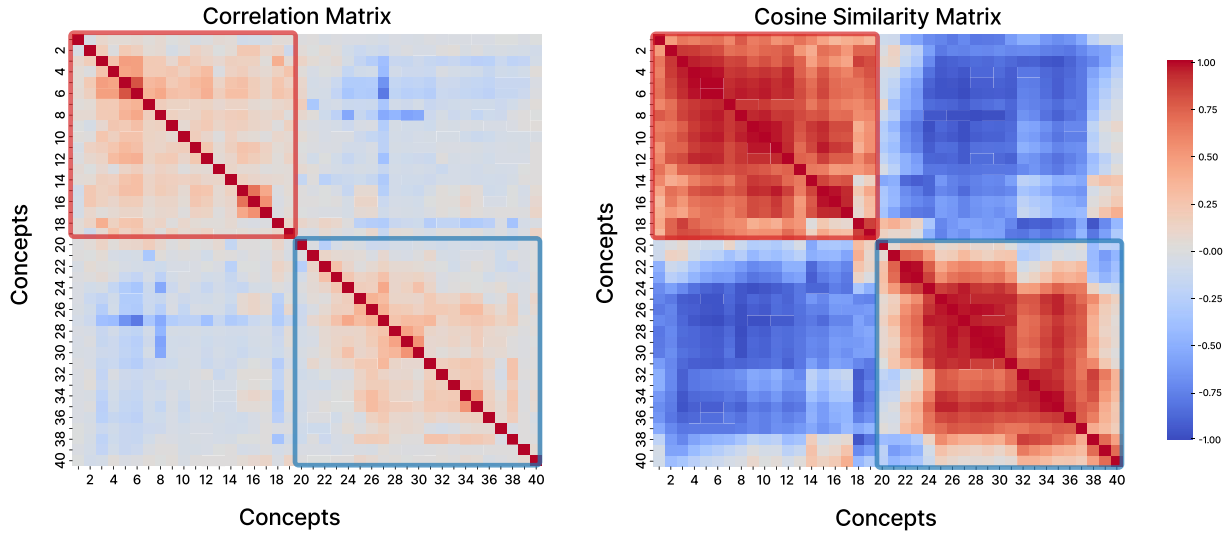


Figure 10: *Left*: Correlation matrix of all concepts in CelebA. *Right*: Cosine similarity matrix of concepts fitted on the last convolution layer of VGG16 trained on CelebA dataset. The two highlighted blocks on both matrices indicate the two natural groups of female (*red*) and male (*blue*) associated concepts.

Index	Concept	Index	Concept	Index	Concept
1	Pale Skin	15	High Cheekbones	29	Goatee
2	Oval Face	16	Smiling	30	Sideburns
3	Attractive	17	Mouth Slightly Open	31	Wearing Necktie
4	Arched Eyebrows	18	Young	32	Receding Hairline
5	Heavy Makeup	19	Big Lips	33	Bald
6	Wearing Lipstick	20	Brown Hair	34	Double Chin
7	Wavy Hair	21	Straight Hair	35	Chubby
8	No Beard	22	Black Hair	36	Eyeglasses
9	Wearing Necklace	23	Bushy Eyebrows	37	Wearing Hat
10	Pointy Nose	24	5 o’Clock Shadow	38	Gray Hair
11	Rosy Cheeks	25	Bags Under Eyes	39	Blurry
12	Wearing Earrings	26	Big Nose	40	Narrow Eyes
13	Bangs	27	Male		
14	Blond Hair	28	Mustache		

Table 3: Concept labels present in the CelebA dataset, ordered and colored as in the correlation and cosine similarity matrices (best seen in color).

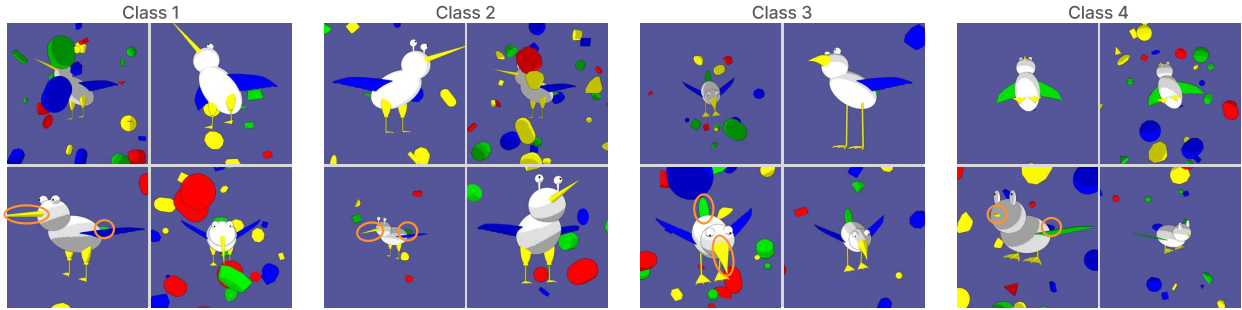


Figure 11: Example samples generated in the first 4 classes of the FunnyBirds dataset. Some examples of concepts with enforced correlations are highlighted.

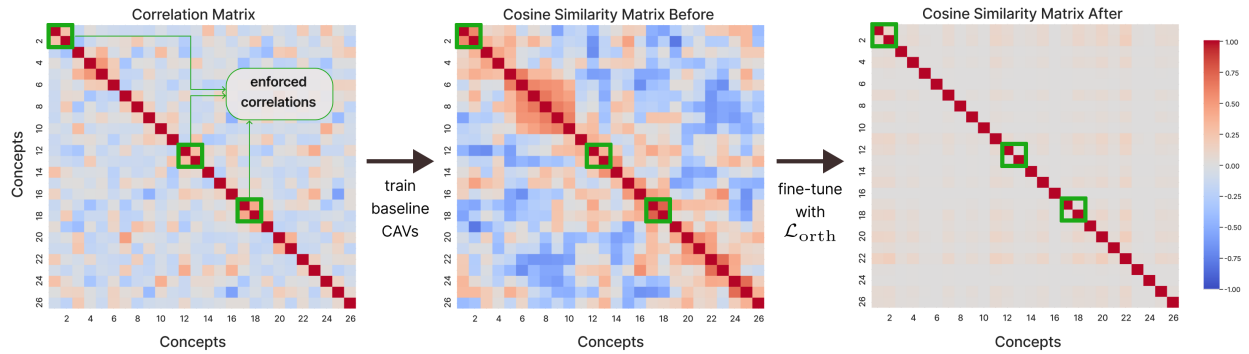


Figure 12: *Left*: Correlations of known concepts based on their co-occurrence in FunnyBirds dataset. *Middle and Right*: Cosine similarity matrices of CAVs, trained on ResNet18 model on the FunnyBirds dataset, before and after the fine-tuning. The highlighted blocks indicate the concept pairs with enforced correlations.